International Journal of Computational Methods and Experimental Measurements
Vol. 13, No. 2, June, 2025, pp. 391-403
Journal homepage: http://iieta.org/journals/ijcmem

Experimental Analysis of Neck Biomechanics Under Dynamic Vehicle Conditions Using a Load Cell-Based Measurement Framework

Waskito Jumali Asni Dawam, Giva Andriana Mutiara*, Muhammad Rizqy Alfarisi

Computer Technology Program Study, School of Applied Sciences, Telkom University Main Campus, Bandung 40257, Indonesia

Corresponding Author Email: givamz@telkomuniversity.ac.id

https://doi.org/10.18280/ijcmem.130216

Received: 1 May 2025
Revised: 12 June 2025
Accepted: 19 June 2025
Available online: 30 June 2025

Keywords:
biomechanics, neck forces, load cell, ergonomics, vehicle safety

ABSTRACT

Neck injuries remain a critical concern in vehicle safety, particularly during dynamic movements and terrain-induced impacts. Traditional test dummies and wearable devices often fail to capture real-time biomechanical neck responses under such conditions. This study introduces a smart mannequin system designed to measure axial forces and cervical moments in realistic vehicle environments. The system integrates S-type load cells and HX711 amplifiers with a Raspberry Pi 4 for real-time processing, enhanced by Kalman filtering for signal clarity. Calibration was conducted using reference weights from 5 N to 40 N in 5 N increments, with each step validated against a force gauge. The mannequin was tested across various terrains, including straight tracks, inclines, sinusoidal roads, and uneven surfaces, representing realistic military and civilian vehicle conditions. Results showed minimal calibration deviation (2–4 N), with peak force measurements reaching 30.63 N and moment readings up to 1.25 Nm. Higher speeds reduced axial loading on stable tracks, while irregular terrain increased neck strain. The system consistently captured neck loading dynamics, offering a safe, repeatable alternative to human-based testing. Its practical application spans ergonomic vehicle design, occupant safety analysis, and fatigue detection in transport environments.

1. INTRODUCTION

Designing environments to meet human needs, a concept central to ergonomics, is vital for ensuring safety and comfort across various domains [1]. From workplace setups to daily tools, ergonomics plays a crucial role in enhancing productivity, reducing physical strain, and preventing injuries [2]. The neck, as a biomechanically sensitive and critical area, often experiences stress and discomfort during routine tasks, highlighting the importance of precise and effective ergonomic solutions [3]. Recent technological innovations, including force-measuring systems, have provided researchers with tools to address these challenges and develop solutions for safer and more comfortable human interactions with their environments [4-7].

Analyzing the neck poses significant challenges due to its intricate biomechanics and susceptibility to dynamic forces [8-13]. Whiplash injuries, for instance, are prevalent in rear-end collisions, often leading to neck pain and associated disorders [14-18]. These injuries are not only common in vehicle crashes but also occur in occupational settings where repetitive or extreme motions strain the cervical spine [19-22]. Additionally, vehicle dynamics like vibrations and sudden accelerations expose the neck to forces that are difficult to measure with precision [23, 24]. Overcoming these obstacles is crucial to developing safety systems that minimize injury risks and enhance comfort for passengers and drivers.

Conventional force measurement methods, including crash test dummies and static models, offer insights but fall short in replicating real-world conditions [25-28]. Wearable sensors add a degree of adaptability but often rely on human test subjects, raising ethical and logistical concerns [29-32]. Recent developments, such as integrating load cells into dynamic systems, enable accurate, real-time force measurements under controlled yet realistic conditions, bridging a crucial gap in current methodologies [33-35].

Several recent studies have attempted to address these limitations using innovative sensor-based approaches. Lin et al. [36] proposed a cervical spine biomechanics evaluation system based on a 3D-printed C2-C3 vertebrae model embedded with flexible pressure sensors, validated through finite element analysis. While their system provided detailed pressure mapping during flexion, extension, and rotation, it was primarily confined to static or robotic test conditions. Other methods, such as strain gauge-based systems [37, 38] and pressure sensors [39], have been explored for their real-time capabilities, but they typically lack depth sensitivity or struggle in highly dynamic environments. Electromyographic (EMG) systems, which measure muscle activity as a proxy for force, offer another alternative but often suffer from signal instability and require complex calibration procedures [40, 41]. These findings highlight the need for a robust, field-

deployable solution capable of directly and reliably measuring neck forces and moments under realistic operational conditions.

This research focuses on creating a neck force-measuring system integrated into a mannequin to provide precise, real-time data during dynamic scenarios. By incorporating advanced load cell sensors and a robust data analysis framework, this system addresses the limitations of traditional approaches. It is designed to deliver practical insights that support enhanced ergonomic evaluations and vehicle safety designs.

The methodology integrates strategically placed load cells, cutting-edge microcontrollers, and an intuitive data visualization platform to deliver a robust force measurement system. This approach not only improves the safety and ergonomics of vehicle designs but also offers a versatile solution adaptable to various industries, making it a significant advancement in applied ergonomics.

The remainder of this paper is organized as follows: Section 2 reviews related work, Section 3 presents the results and discusses the findings, and Section 4 concludes with future directions.

2. RESEARCH METHODS

This section reviews the relevant literature on force measurement technologies, the application of smart mannequins in ergonomic studies, and the challenges associated with neck biomechanics. By identifying key advancements and gaps in the field, this review establishes the foundation for the proposed neck force-measuring system.

2.1 Literature review

Accurate biomechanical force measurement is essential for improving safety and comfort in both vehicle environments and occupational settings. Among the most vulnerable areas of the human body is the neck, which supports the weight of the head while allowing a wide range of motion. Its complex biomechanics make it particularly susceptible to dynamic loads, especially during real-world scenarios such as off-road driving, uneven terrain traversal, or long-term exposure to vibration [42-44]. These forces, though often less severe than crash impacts, can still produce chronic musculoskeletal issues over time [45].

One of the most prevalent cervical injuries in vehicle environments is whiplash, commonly caused by sudden acceleration-deceleration forces, such as in rear-end or side-impact collisions [11, 46]. This condition is characterized by hyperflexion and hyperextension of the neck, often resulting in soft tissue damage, inflammation, and long-term pain. Beyond whiplash, individuals exposed to continuous low-level vibration—such as military personnel, construction vehicle operators, or long-haul drivers—may develop cumulative trauma disorders [47, 48]. These include cervical strain, degenerative disc changes, and tension-type neck pain. Occupational settings involving awkward postures or repetitive tasks, such as aviation maintenance or heavy machinery operation, have also been linked to increased risk of chronic neck discomfort [49]. Capturing the mechanical origins of these injuries requires systems that can detect not only sudden force spikes but also sustained loading and subtle moment variations over time [50].

These injury patterns highlight the limitations of traditional testing tools like crash test dummies (anthropomorphic test devices), which have long served as the standard in vehicle safety evaluation [51]. However, they are primarily engineered for high-speed collision scenarios, offering limited insight into lower-intensity, repetitive motions typical of operational driving conditions. Their rigid neck structures, limited joint articulation, and sparse sensor configurations restrict their ability to simulate or capture cervical dynamics in real time [52, 53]. Likewise, static models—though useful for anthropometric or postural analysis—are incapable of replicating time-dependent force interactions or movement feedback under dynamic conditions. These limitations have left a significant gap in real-time cervical force monitoring for ergonomic research [54].

To address these challenges, researchers have explored a variety of alternative sensors. Electromyography (EMG) has been used to estimate muscle activation, but its indirect nature and high signal variability limit its accuracy [55]. Pressure sensors, while simple to apply, are primarily suited for surface interactions and lack depth sensitivity [56]. Strain gauges provide localized strain data but are sensitive to environmental drift and difficult to install in moving systems [57]. Each of these systems presents constraints that make them less ideal for dynamic neck force measurement.

In contrast, load cells offer direct, real-time force measurements with high accuracy and minimal noise [58]. Their robustness under motion, compatibility with dynamic systems, and adaptability for field and lab settings make them particularly suitable for capturing axial loads and calculating neck moments. When integrated into a mannequin structure, load cells enable the simulation and monitoring of neck biomechanics under realistic conditions. Table 1 summarizes the comparative advantages and limitations of commonly used sensor types in this domain.

Table 1. Comparative overview of sensor technologies for cervical biomechanics

Sensor Type	Advantages	Limitations
EMG	Captures neuromuscular response	Indirect measurement, high variability, signal noise [59]
Pressure Sensor	Easy to apply, good for interface force detection	Lacks directionality and depth information [60]
Strain Gauge	High sensitivity in controlled conditions	Installation complexity, temperature-sensitive [61]
Load Cell	High accuracy, real-time output, reliable in dynamic settings	Requires mechanical integration; limited to specific axes

These constraints underscore the need for a dedicated, responsive system capable of capturing real-time neck loading in both controlled and realistic environments. The smart mannequin developed in this study addresses this gap by integrating load cell technology with a biomechanically responsive neck structure. Its use in both laboratory and field tests provides a novel approach for tracking cervical forces and moments, offering greater fidelity, repeatability, and ethical safety compared to traditional human-subject methods.

2.2 System design

The primary objective of this system is to measure forces

applied to the head and the moments generated by neck movements when subjected to uneven terrain. This functionality is achieved by utilizing load cells to detect the forces and employing a custom mechanical setup to capture the moments caused by neck movement.

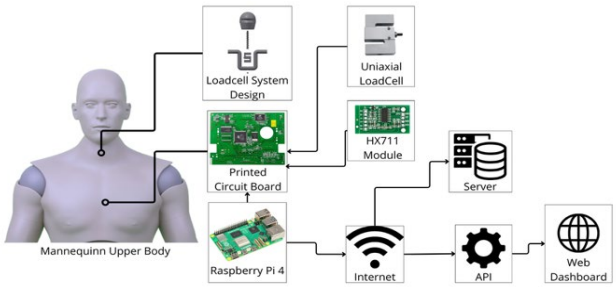

Figure 1. System design of neck measurement system

The system which can be seen on Figure 1 relies on S-type uniaxial load cells to measure the forces exerted on the head. These sensors are connected to HX711 amplifiers, which process the signals for accurate data acquisition. The load cells are strategically positioned beneath the neck within the chest section of the mannequin to ensure precise measurements of the forces transmitted through the neck structure.

As a fundamental concept in biomechanical analysis, the applied force on the mannequin is described by Newton's Second Law, as shown in Eq. (1):

$$F = m \cdot a \tag{1}$$

where, F represents the force (N), m is the mass (kg) acting on the system, and a is the acceleration (m/s²) resulting from dynamic motion. This equation forms the theoretical basis for interpreting the forces exerted on the neck during testing, particularly in scenarios involving varying speeds and terrain-induced vibrations.

A Raspberry Pi 4 serves as the primary microcontroller, managing both data acquisition and processing tasks. Its computational capacity enables efficient handling of real-time sensor data and seamless communication with the visualization platform. The system is powered by a portable power bank, providing flexibility and ensuring uninterrupted operation independent of external power sources. Data transmission occurs via Wi-Fi and an API, allowing real-time sensor readings to be sent to a web-based dashboard. This dashboard facilitates the visualization of both real-time and historical data, offering insights into the forces and moments experienced by the mannequin's neck.

To evaluate the moments acting on the neck (flexion, extension, and lateral), the system applies the basic principle of rotational mechanics. As shown in Eq. (2), the moment of force is calculated as the product of the applied force and the perpendicular distance from the axis of rotation to the point of force application. The moment of force is defined as:

$$M = d \cdot F \tag{2}$$

Here, M represents the moment (Nm), F is the axial force measured by the load cell (N), and d is the perpendicular distance from the point of force application (e.g., the contact point on the head or neck) to the axis of rotation (m). In the proposed setup, this distance is determined based on the geometric configuration of the spring-loaded U-joint structure connecting the mannequin's head and neck. By applying known lateral and axial forces at fixed offsets, the system approximates neck moments in dynamic scenarios.

To better visualize the physical interpretation of Eq. (2), a simplified biomechanical model of the neck is presented in Figure 2. The mannequin's head is modelled as a rigid body pivoting at the base of the neck. External forces applied at a distance d from this pivot produce mechanical moments corresponding to flexion, extension, or lateral bending, depending on the direction of the applied force.

This model clarifies how sensor data and known offsets can be mapped to real-world neck mechanics. The schematic complements the physical structure shown in Figure 2 by illustrating the force–moment relationship in biomechanical terms.

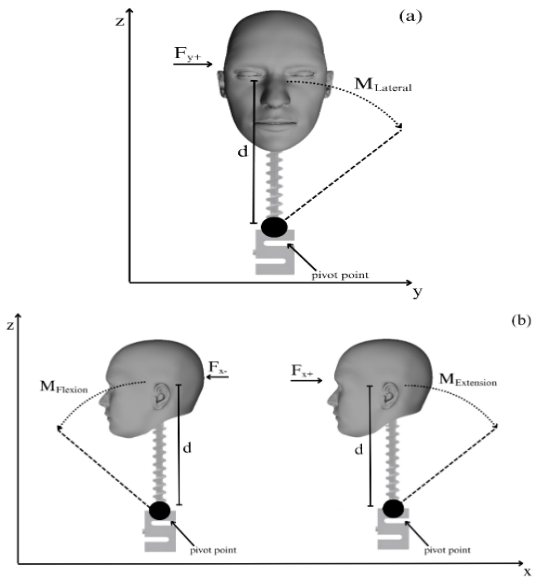

Figure 2. Lateral, flexion and extension moments, (a) Lateral bending moment produced by side-directed force on the head, (b) Flexion and extension moments produced by anterior and posterior force application on the head

The value of d corresponds to the offset distance in the spring-mounted U-pipe assembly illustrated in Figure 2 which connects the arms and houses the load cell at the midpoint of the U-structure. A motorcycle spring is positioned on top of the load cell, enabling controlled head movement while accurately transmitting forces and moments to the sensor. Calibration of the load cell sensors is performed prior to use by placing a known weight on the system. A dedicated software program facilitates this process, ensuring the sensor readings align with the expected values of the reference weight. Data captured by the sensors is stored locally on the Raspberry Pi's internal storage when Wi-Fi is unavailable. In the presence of Wi-Fi, the data is transmitted to the web dashboard via the API. This dual approach ensures data accessibility and reliability under varying connectivity conditions. Although specific durability measures are not currently implemented, the modular design of the system provides opportunities for future enhancements to improve its resilience in demanding environments.

The system has undergone initial laboratory testing to verify its ability to measure forces accurately. Known weights were

used to validate the calibration of the load cells. Additionally, preliminary tests were conducted to assess the moments generated by neck movements during development. While the system demonstrated reliable force measurement capabilities, external validation tools for moment calculations were unavailable. Future efforts may involve the development or integration of specialized tools to enhance validation.

While load cells provide accurate, real-time force measurements, their integration into a dynamic mannequin system introduces several practical challenges. Mechanical alignment is critical; misalignment between the mannequin's neck structure and the load cell can introduce off-axis forces, resulting in inaccurate readings. The uniaxial nature of S-type load cells also limits their ability to detect complex multi-directional forces unless complemented with additional sensors. Furthermore, ensuring secure sensor placement in a movable, jointed system requires careful design to avoid mechanical decoupling or slippage during movement. Electrical wiring must be strain-relieved and shielded to minimize noise and disconnection due to repeated motion. Temperature changes and prolonged use may also lead to signal drift or require periodic recalibration. These factors were considered in the mechanical design, and while initial testing confirmed functional stability, future improvements will focus on enhancing mounting robustness and environmental resilience.

2.3 System flowchart

The physical design of the neck–head measurement structure is illustrated in Figure 3, which shows the mannequin head, motorcycle spring, and U-shaped PVC component. This setup serves as the mechanical basis for capturing forces and moments during motion, with the load cells mounted to respond to movement and pressure along the vertical axis.

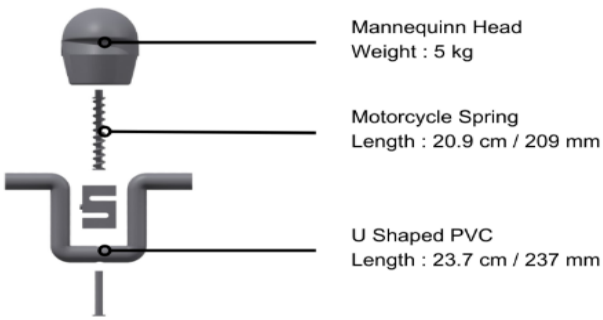

Figure 3. Neck to head structure

The flowchart as seen in Figure 4 represents the operational workflow of the proposed neck force-measuring system. It outlines the sequential steps involved in initializing the system, acquiring and processing data, and ensuring its accessibility for further analysis. The flowchart serves as a visual guide to understand the system's logic and decision-making processes, ensuring clarity and reproducibility in its implementation.

The process begins with the initialization of the Raspberry Pi microcontroller, ensuring that all hardware and software components are properly configured and ready for operation. Following this, the system performs a self-calibration process for the load cells, a vital step to ensure accurate force measurements. During calibration, the sensor readings are adjusted to align with predefined reference values, minimizing any potential errors.

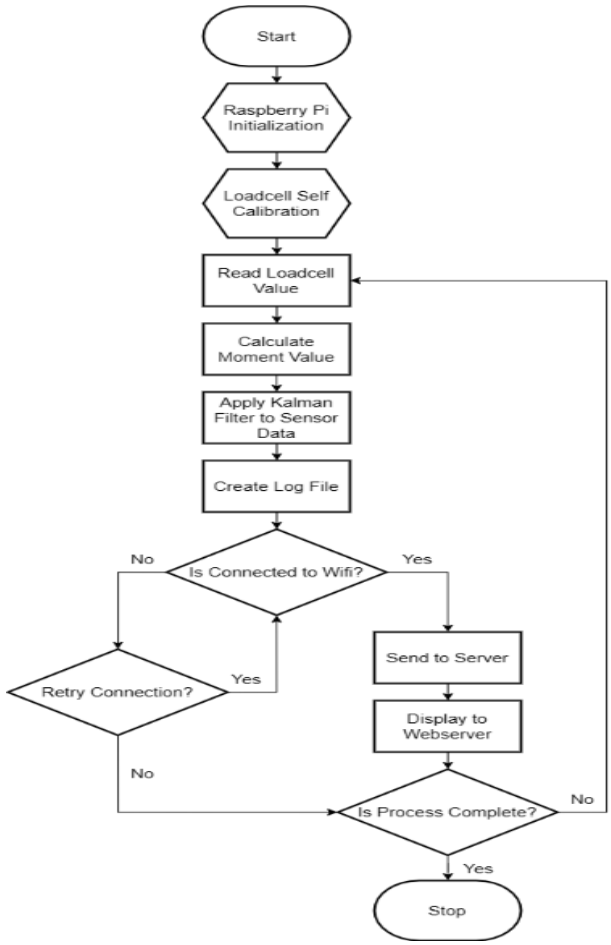

Figure 4. Flowchart of force and moment measurement system

After calibration, the system proceeds to acquire real-time data from the load cells. This raw data is processed using a Kalman filter algorithm with Eqs. (3)-(5), which reduces noise and improves accuracy. The Kalman filter operates using the following equations:

$$K_k = \frac{P_{k-1}}{P_{k-1} + R} \tag{3}$$

where, K_k is the Kalman gain, P_{k-1} is the process variance, and R is the measurement variance.

The updated state estimate is then computed as:

$$x_k = x_{k-1} + K_k \cdot (z_k - x_{k-1}) \tag{4}$$

where, x_k is the updated state (filtered estimate), x_{k-1} is the Previous state estimate, and z_k is the new measurement.

The updated process variance is calculated as:

$$P_k = (1 - K_k) \cdot P_{k-1} \tag{5}$$

After calibration, the system proceeds to acquire real-time data from the load cells. This raw data is processed using a Kalman filter, which reduces noise and improves accuracy. Once processed, the data is logged into local storage, creating a secure record that ensures accessibility even in the absence of network connectivity. This dual functionality guarantees that the collected data remains retrievable for further analysis regardless of the system's connectivity status.

One of the critical decision-making steps in the workflow involves checking for Wi-Fi connectivity. If the system detects an active Wi-Fi connection, it transmits the processed data to a server, enabling visualization on a web-based dashboard. This dashboard provides users with real-time monitoring and analysis of the neck forces and moments experienced by the mannequin. If no Wi-Fi connection is available, the system securely retains the data in its local storage for later retrieval and use.

At the end of each operational cycle, the system evaluates whether further measurements are required. If additional data collection is necessary, the process loops back to the data acquisition stage, allowing for continued operation. If the operation is complete, the system shuts down, effectively concluding the cycle. This logical progression ensures efficient use of resources while maintaining data integrity.

The Wi-Fi connectivity check is a critical feature of the system, enabling flexible and reliable operation under varying network conditions. Similarly, the evaluation of the operational cycle's completion ensures that the system efficiently transitions between tasks or concludes its workflow when appropriate. These decision points are integral to maintaining the adaptability and efficiency of the system's operation.

The system's outputs include real-time data visualization on the web-based dashboard, which allows users to evaluate the mannequin's performance under various conditions. Additionally, the system's ability to log data locally on the Raspberry Pi provides an essential offline storage option, ensuring that data remains accessible for further analysis when network access is unavailable. The flowchart provides a comprehensive representation of the system's operational logic. Each step is carefully designed to ensure accurate and reliable data acquisition and processing. By incorporating decision points such as Wi-Fi connectivity and operation completion, the system demonstrates robustness and adaptability in diverse operational conditions. The application of the Kalman filter enhances data quality, while the dual data storage capability ensures redundancy and reliability. These features collectively make the system a practical and effective tool for ergonomic analysis and safety assessments.

2.4 Testing scenarios

The purpose of the testing scenarios was to validate the accuracy of the system's force and moment measurements under real-world conditions. Unlike simulation-based approaches, this study relied on empirical data collected directly from field trials, ensuring realistic representation of vehicle-induced motion and neck loading. These tests were conducted in two distinct environments: the Test Tracks and Uneven Terrain. The dataset consisted of 20 distinct test conditions, combining six terrain types and varying speed levels, with each condition contributing seven consecutive data points from real-world vehicle testing. This approach ensures the dataset accurately reflects dynamic motion while maintaining consistency for analysis. In addition, two slope scenarios—uphill at 45% and downhill at 60%—were tested under dynamic, non-standardized speeds to assess the system's performance during extreme gradient transitions. Both environments were chosen to challenge the system's ability to capture and process data in conditions simulating the dynamic movements and shocks experienced by a neck in a rugged vehicle.

The laboratory testing aimed to calibrate the load cells and validate their performance in a controlled setting. To achieve this, the system was calibrated using known reference weights ranging from 5 N to 40 N, applied in 5 N increments to the top of the mannequin's head to simulate axial force. At each increment, the load cell's output was compared against a pre-calibrated handheld force gauge, ensuring reliable ground-truth validation. A custom Python-based script mapped the raw ADC values from the HX711 module to real-world force values, forming a calibration curve with a strong linear response. Deviations between load cell and force gauge readings were observed to be within 2-4 N at higher loads. To quantitatively evaluate this deviation across all calibration points, the accuracy was further assessed using the Mean Error Percentage (MEP), calculated as:

$$MEP = \frac{1}{n}\sum_{i=1}^{n}\left|\frac{F_{Gauge,i} - F_{Loadcell,i}}{F_{Gauge,i}}\right| \times 100 \qquad (6)$$

where, n is the number of measurement samples, $F_{Gauge,i}$ is the force measured by the force gauge in the i^{th} trial, and $F_{Loadcell,i}$ is the corresponding load cell measurement. This metric provided a more detailed assessment of calibration quality beyond single-point deviations, reinforcing the reliability of the system under expected force ranges.

This metric confirmed that error rates remained within an acceptable range (MEP$\approx$3.12%), supporting the validity of the calibration. For moment validation, controlled lateral, flexion, and extension forces were applied at known distances from the neck pivot point. The corresponding moment values were computed using torque equations and compared with sensor outputs to ensure consistency. This combined calibration and validation approach confirmed that the system maintained reliable accuracy across its expected force and moment ranges.

The Test Tracks, a specialized vehicle testing facility, offered various road types and conditions for dynamic system evaluation. The tests included measurements on a straight road at speeds of 10 to 40 km/h, where the system demonstrated consistent force readings, with minor variations caused by vehicle vibrations at higher speeds. Inclined tracks, tested at similar speeds, revealed the system's sensitivity to gravitational loads, with forces increasing proportionally to the gradient.

Sinusoidal bumps (Sinus 1 and Sinus 2) introduced oscillatory forces, providing a dynamic challenge that allowed the system to demonstrate its capability in capturing transient forces. Parallel blocks created sharp impacts, testing the system's response to high-magnitude forces and moments during rapid transitions. Steep slopes, with gradients of 60% and 35%, allowing for a comprehensive evaluation of the system's accuracy in capturing forces and moments during abrupt changes in gravitational load.

The Uneven Terrain presented a challenging real-world environment with uneven roads to evaluate the system's adaptability. These tests focused on the system's performance during uphill and downhill navigation at speeds of 5 to 15 km/h. The terrain simulated unpredictable forces and moments, offering valuable insights into the system's behavior under off-road conditions.

Throughout all tests, the system collected data on the forces and moments experienced by the mannequin's neck. A Kalman filter was applied to process the raw sensor readings,

refining the output and minimizing noise. This technique enhanced data accuracy and allowed for more reliable analysis of forces and moments. Although no direct comparisons were made with external benchmarks, the data provided critical insights into the system's functionality. The system demonstrated high accuracy in capturing neck forces, particularly during tests at the Test Tracks. However, reduced sensitivity in moment readings was observed under specific conditions, such as during shocks from sinusoidal bumps. Despite these limitations, the system's overall performance remained consistent, and the collected data proved valuable for further analysis and system improvement.

One notable challenge encountered during testing was the reduced sensitivity of the moment readings under certain dynamic conditions, such as shocks experienced on the tracks. This limitation underscores the need for adjustments in sensor placement or calibration to improve moment detection accuracy. Overall, the testing scenarios provided a comprehensive evaluation of the system's capabilities, establishing a strong foundation for refinement and application in dynamic environments.

3. RESULTS AND DISCUSSIONS

This section presents the results obtained from testing the proposed neck force-measuring system and discusses the implications of the findings. The results validate the system's performance under varying conditions and highlight key insights into its accuracy and adaptability.

3.1 Results

The findings from the testing scenarios provide an in-depth understanding of the system's performance under both controlled laboratory conditions and dynamic field environments. The analysis covers axial force measurements and moments of force for flexion, extension, and lateral movements, derived from laboratory testing, the Test Track, and the Uneven Terrain.

The first scenario is laboratory testing results. As seen in Figure 5, a comparison chart illustrates the system's calibration precision, showing that at a force gauge reading of 30 N, the load cell reading without filtering was 27.65 N, while the Kalman-filtered value improved to 29.42 N.

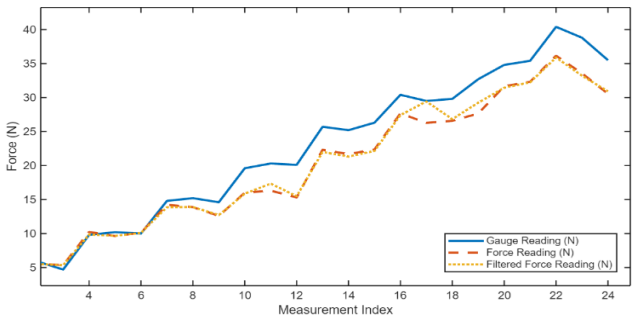

Figure 5. Loadcell measurement index

The axial force readings highlight the accuracy of the load cell system when compared to the force gauge. The load cell readings closely aligned with the force gauge values, with deviations ranging from 2 to 4 N at higher forces (above 15 N). After applying the Kalman filter, the readings demonstrated improved stability and accuracy by minimizing noise in the raw load cell data.

Table 2. Flexion laboratory test results

Force Applied (N)	Average Flexion (Nm)	Average Filtered Flexion (Nm)
5	0.14	0.13
10	0.08	0.07
15	0.23	0.27
20	0.05	0.05
25	0.07	0.10

Table 3. Extension laboratory test results

Force Applied (N)	Average Extension (Nm)	Average Filtered Extension (Nm)
5	0.07	0.07
10	0.02	0.02
15	0.07	0.07
20	0.12	0.12
25	0.14	0.14

Table 4. Lateral moment test results

Force Applied (N)	Average Lateral (Nm)	Average Filtered Lateral (Nm)
5	0.01	0.03
10	0.06	0.06
15	0.09	0.32
20	0.07	0.13
25	0.09	0.09

The measured moments for flexion, extension, and lateral motion were computed using Eq. (2), based on the force values obtained from the load cells and the known offset distance from the rotation axis.

Next, flexion tests result as seen in Table 2 revealed a consistent pattern in the moments of force generated as the applied load increased. For example, at an applied force of 20 N, the flexion moment was recorded at 0.05 Nm both before and after Kalman filtering, demonstrating the system's stability in measuring flexion moments. However, the absence of external validation tools limited the direct assessment of absolute accuracy.

In extension tests as shown in Table 3, the measured moments increased proportionally with the applied force. At a force of 30 N, the extension moment was recorded as 0.25 Nm for raw and 0.273 Nm filtered data. The consistency between raw and filtered values validates the robustness of the system in measuring extension moments under controlled conditions.

Table 4 shows lateral moments, smaller magnitudes of force and moment were observed compared to flexion and extension. At 30 N applied force, the lateral moment was calculated at 0.15 Nm both the raw data and with Kalman filter. These findings confirm the system's ability to measure lateral moments accurately.

Moreover, the test track provided a controlled environment to assess the system's response under different dynamic conditions, particularly on a straight road where external disturbances were minimal. As shown in Figure 6, the recorded force values exhibited a decreasing trend as speed increased. At 10 km/h, the highest force measured was 0.23 N, indicating a relatively higher level of interaction between the mannequin and the vehicle. As speed increased to 20 km/h, the force significantly dropped to 0.04 N, suggesting a

stabilization effect. However, at 30 km/h, a slight increase to 0.13 N was observed, which may be attributed to minor oscillations or variations in road contact. At the highest speed of 40 km/h, the force value reached its minimum at 0.01 N, implying that higher speeds resulted in smoother motion dynamics and reduced vertical displacement. This overall trend suggests that on a straight and smooth surface, the forces exerted on the mannequin decrease as speed increases, likely due to improved stability and reduced impact from surface irregularities. Additionally, the neck moment analysis on a straight road showed no measurable forces acting on the mannequin's neck, confirming a stable head and neck posture with minimal biomechanical strain.

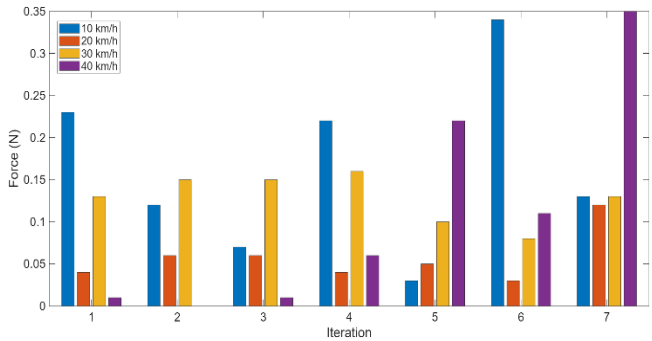

Figure 6. Straight road force test results

The force values observed under dynamic testing conditions reflect the accelerative effects described by Newton's Second Law in Eq. (1), where variations in vehicle speed and surface topology result in corresponding changes in net force exerted on the mannequin's structure. Specifically, when the vehicle encounters inclines, declines, or irregular terrain, the resulting acceleration or deceleration affects the magnitude of force transmitted through the mannequin's neck. These external mechanical inputs directly influence the sensor readings, validating the relationship between motion-induced acceleration and measured force as predicted by fundamental biomechanical principles.

Under the Inclined Road condition as seen in Figure 7, the forces displayed a gradual increase with speed before slightly declining. At 10 km/h, the recorded force was 0.01 N, increasing to 0.03 N at 20 km/h and peaking at 0.17 N at 30 km/h. However, at 40 km/h, the force dropped slightly to 0.11 N. This pattern indicates that as the vehicle maneuvers on an inclined surface, higher speeds amplify the forces, but the decline at higher speeds may reflect reduced lateral force impact due to stabilization effects.

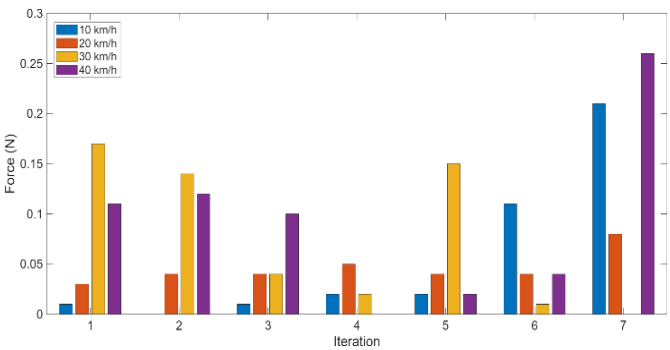

Figure 7. Inclined Road force test results

The results from the Inclined Road test indicate uniform neck moment values across all movement directions. Figure 8. shows recorded values for flexion, extension, and lateral movements are all 0.143 Nm for both raw and filtered data, showing no significant variation. The identical values across all directions suggest a balanced distribution of forces during tilting motion. Additionally, the absence of fluctuations between raw and filtered data indicates minimal noise interference, ensuring high reliability of the measurements. These findings highlight that the tilting motion results in consistent neck loading, which may suggest a stable posture adaptation without excessive strain on any specific direction.

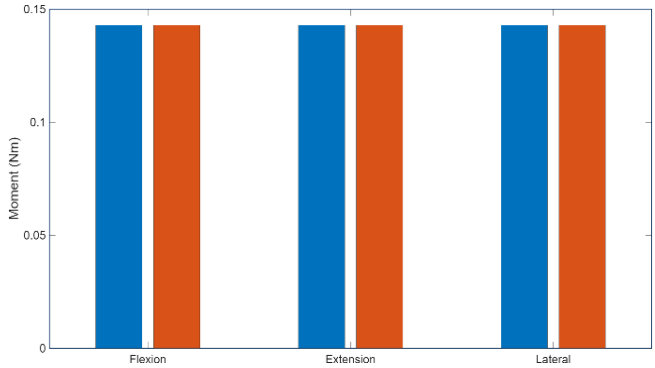

Figure 8. Inclined track moment test results

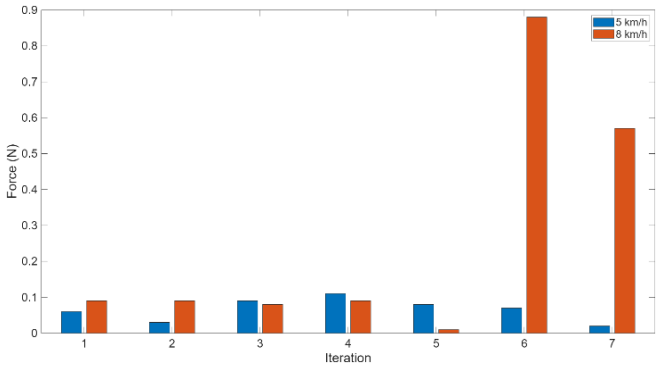

Figure 9. Sinusoidal-1 force test results

The sinusoidal road conditions reveal distinct force responses. For Sinusoidal 1 Road as seen in Figure 9, the forces were higher at lower speeds, with values of 0.06 N at 5 km/h and 0.09 N at 8 km/h, reflecting a direct impact of the undulating surface on the force measurements.

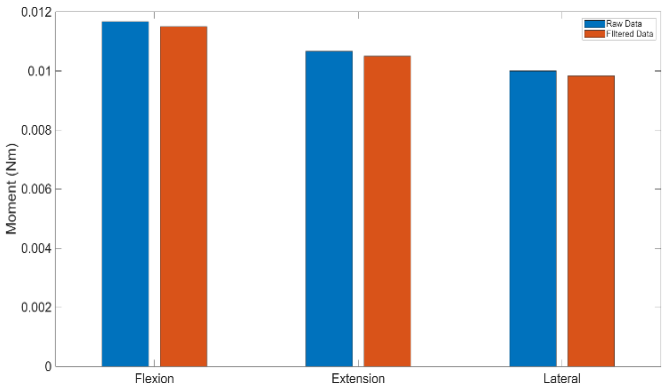

Figure 10. Sinusoidal-1 moment test results

The results from the Sinusoidal-1 test which can be seen in Figure 10 indicate relatively low neck moment values across all measured directions, suggesting minimal strain during this motion. The raw flexion moment was recorded at 0.01167 Nm, with a filtered value of 0.0115 Nm, indicating minimal noise in the measurements. Similarly, the extension moment showed values of 0.01067 Nm (raw) and 0.0105 Nm (filtered), while the lateral moment recorded 0.01 Nm (raw) and 0.00983 Nm (filtered). The filtered values closely follow the raw data, confirming the consistency of the measurements. These results suggest that Sinusoidal 1 moments induces minimal neck loading, likely due to controlled movements and stable posture during this phase. The low magnitude of forces implies that this motion does not contribute significantly to neck strain, making it a relatively neutral movement in terms of biomechanical impact.

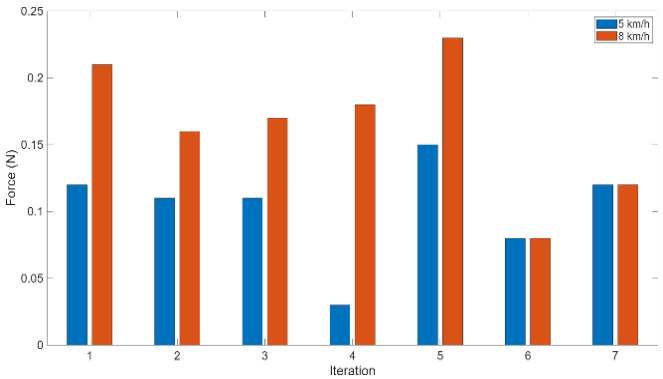

Figure 11. Sinusoidal-2 force test results

In sinusoidal-2 Road, as seen in Figure 11, the force magnitudes were broader, ranging from 0.12 N at 5 km/h to 0.21 N at 8 km/h, showing a greater dynamic response compared to Sinus1. These results emphasize the pronounced effect of sinusoidal bumps on the mannequin's force readings, especially as the surface undulations increase in intensity. The increased force variations suggest that as the vehicle moves over periodic bumps, the mannequin experiences more fluctuations in vertical displacement, resulting in higher recorded forces. This could be attributed to the oscillatory motion of the surface, which amplifies dynamic effects on the mannequin's load sensors. The more pronounced forces at higher speeds highlight the impact of increased kinetic energy in response to surface irregularities, making sinusoidal road profiles a critical factor in assessing biomechanical stability. Additionally, the analysis of neck moments revealed no measurable forces acting in flexion, extension, or lateral directions, suggesting that the mannequin's head and neck remained stable despite the oscillatory motion.

The parallel blocks test revealed notable force variations across different speeds, as depicted in Figure 12. At a low speed of 5 km/h, the force recorded was 0.08 N, indicating minor disturbances due to the structured obstacles. However, as speed increased to 8 km/h, the force surged to 0.91 N, reflecting the more pronounced impacts caused by the rigid parallel blocks. This pattern suggests that as velocity rises, the mannequin encounters more intense and frequent force spikes due to the structured and repetitive nature of the obstacles. The test highlights the system's capability to capture sudden changes in surface conditions, demonstrating its responsiveness to rapid, uneven shocks. The parallel arrangement of obstacles produced a repetitive force pattern, which underscores the mannequin's sensitivity to abrupt load changes, particularly at higher speeds. Despite these variations, analysis of neck moments, showed no measurable torque in any direction, indicating that the mannequin's head and neck remained stable, unaffected by the parallel block-induced disturbances. The absence of neck moment values could be attributed to the test setup's suspension system effectively absorbing vibrations before they reached the mannequin or to the mannequin's inherent resilience against minor perturbations.

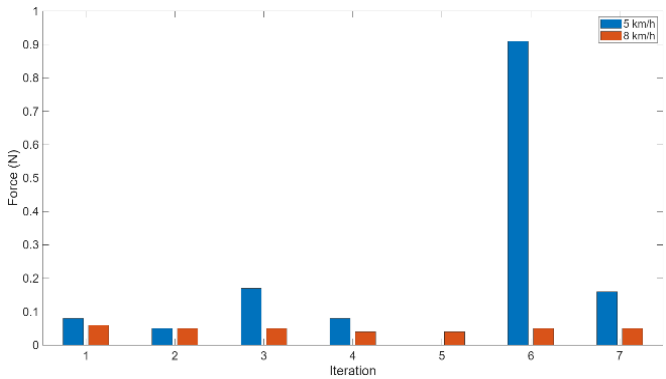

Figure 12. Parallel blocks force test results

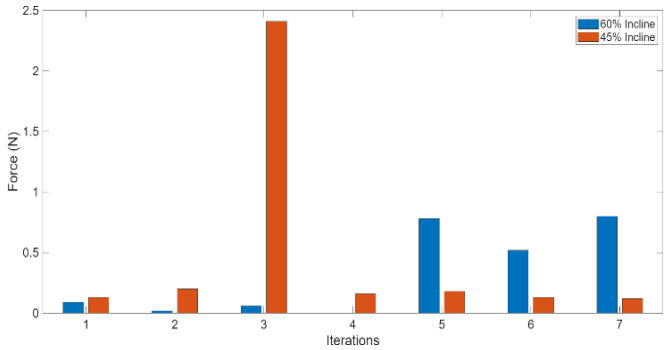

Figure 13. Inclined Road force test results

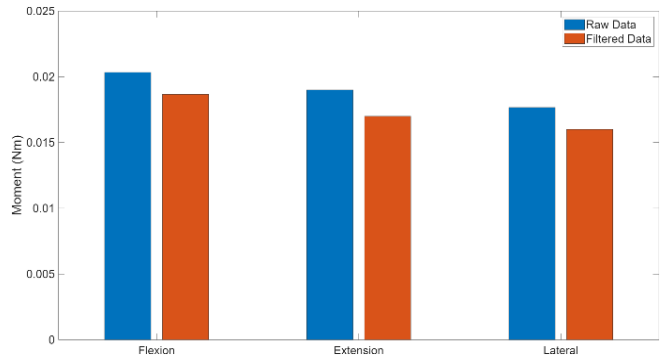

Figure 14. 45% Incline moment test results

The 45% uphill slope test conditions demonstrated a gradual increase in force values as the slope's steepness and speed combined in Figure 13. The force started at 0.09 N and reached a peak of 0.78 N, highlighting the effect of gravitational pull and vehicle dynamics during uphill motion. As the mannequin experienced greater pressure, the force steadily increased with speed, indicating a more predictable loading pattern. In contrast, in Figure 14, the 60% downhill condition showed significant fluctuations in force values, with a dramatic peak of 2.41 N at 30 km/h before dropping to 0.16 N at 40 km/h.

This sharp variation suggests that acceleration and shifting load dynamics contribute to amplified forces during descent. Despite these force variations, the mannequin's neck remained stable on the 60% incline, with no measurable moments in flexion, extension, or lateral directions. However, the 45% incline test recorded small but consistent neck moments across all directions, with flexion showing the highest values.

The results from the uphill testing at Uneven Terrain as seen in Figure 15, conducted at speeds of 5 to 15 km/h, reveal distinct trends in the forces experienced by the mannequin. At the lowest speed of 5 km/h, forces are consistently high, averaging at 4.94 N, reflecting the significant gravitational and terrain-induced resistance during the climb. As the speed increases to 10 km/h, there is a noticeable reduction in force magnitudes, with values reaching 0.37 N in average. This reduction suggests that the higher speed reduces the duration of terrain contact, minimizing the impact forces. At 15 km/h, the forces begin to rise again, ranging from 1.01 N to a maximum of 5.03 N, indicating that the increased speed amplifies the dynamic effects of the uneven terrain on the mannequin. The variations in forces across these speeds highlight the system's sensitivity to both gravitational pull and the dynamic interaction between vehicle motion and terrain characteristics, offering valuable insights for assessing neck and body load distribution in challenging environments.

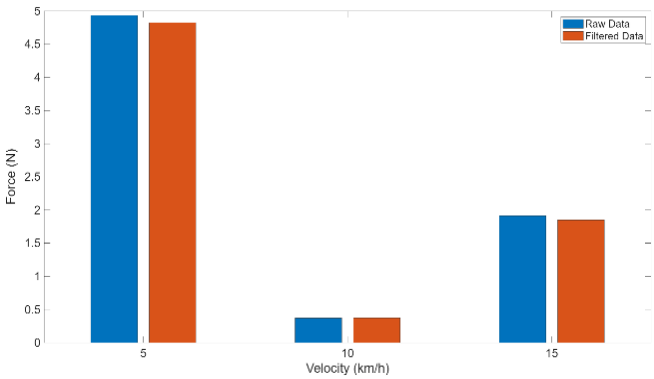

Figure 15. Uphill force test results

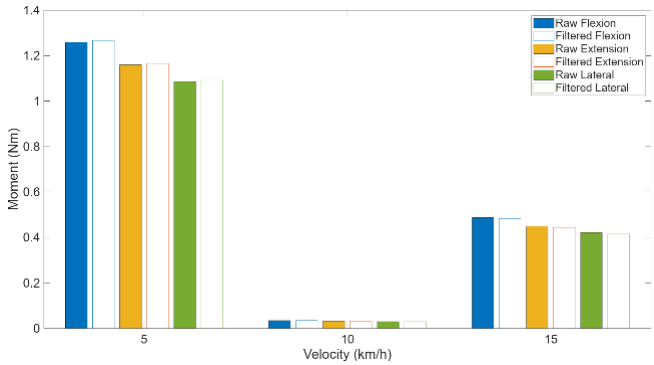

Figure 16. Uphill moment test results

The results of the uphill motion tests, as illustrated in Figure 16, indicate that neck moments vary significantly with velocity. At 5 km/h, the mannequin experienced the highest forces, with flexion, extension, and lateral moments averaging 1.258 Nm, 1.16 Nm, and 1.086 Nm, respectively. This suggests that at lower speeds, the mannequin encounters greater resistance forces, likely due to the initial effort required to overcome inertia. However, at 10 km/h, all moment values dropped drastically to approximately 0.034 Nm (flexion), 0.032 Nm (extension), and 0.029 Nm (lateral), indicating that at moderate speeds, the mannequin maintains a more stabilized posture, reducing strain on the neck. At 15 km/h, the values increased again, with flexion, extension, and lateral moments reaching 0.49 Nm, 0.45 Nm, and 0.42 Nm, respectively. This moderate increase suggests that higher speeds introduce additional dynamic instability, leading to slight fluctuations in neck loading. These findings highlight that lower speeds tend to generate higher neck moments due to initial resistance, whereas moderate speeds provide the most stable conditions, and higher speeds cause a slight rise in forces due to acceleration effects.

Meanwhile the results from the downhill testing at Uneven Terrain highlight significant variability in the forces experienced by the mannequin due to the dynamic nature of the descent. In Figure 17, the lowest force readings, values ranged from 0.06 N to 0.37 N and averaging at 1.32 N, corresponding to minimal resistance and smoother terrain sections. However, extreme spikes were observed, such as a peak force of 30.63 N, reflecting sudden impacts or jolts likely caused by abrupt terrain changes or increased gravitational acceleration during steeper sections of the slope. At moderate force levels, values consistently ranged between 1.06 N and 2.70 N, representing sections where the vehicle-maintained stability while navigating uneven terrain. Additionally, lower force peaks such as 4.89 N and 4.68 N indicate sections of controlled descent with moderate terrain irregularities.

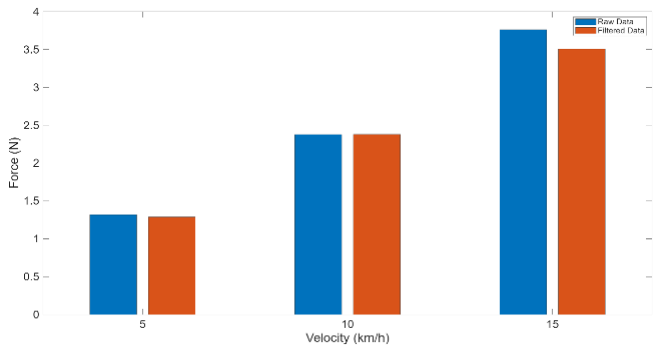

Figure 17. Downhill force test results

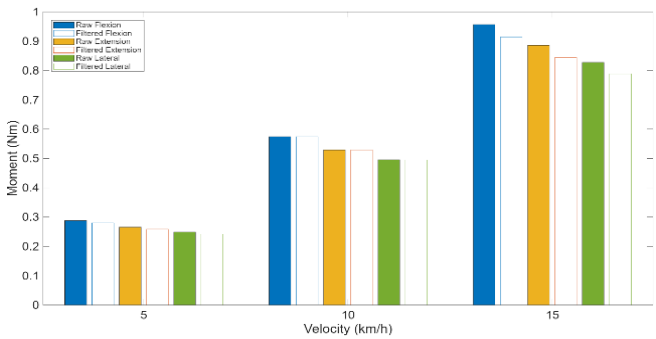

Figure 18. Downhill moment test results

The results of the downhill moment tests, as seen in Figure 18, reveal a trend of increasing neck moments with higher velocities. At 5 km/h, the mannequin experienced relatively low forces, with flexion, extension, and lateral moments averaging 0.29 Nm, 0.27 Nm, and 0.25 Nm, respectively. This suggests that at lower speeds, the gravitational force assists the movement, reducing the strain on the neck. However, as the velocity increased to 10 km/h, the moment values nearly doubled, with flexion, extension, and lateral moments

reaching 0.57 Nm, 0.53 Nm, and 0.50 Nm, respectively. This indicates that at moderate speeds, the mannequin experiences greater dynamic forces, likely due to increased momentum and the need for postural adjustments. At 15 km/h, the forces rose further, with flexion, extension, and lateral moments recorded at 0.96 Nm, 0.89 Nm, and 0.83 Nm, respectively. This significant increase suggests that higher speeds introduce greater instability and require higher muscular effort to maintain posture and control movement. These findings indicate that downhill motion results in progressively higher neck loading as speed increases, highlighting the importance of speed control in ergonomic and biomechanical assessments to minimize excessive strain on the neck.

3.2 Discussions

The purpose of this study was to evaluate whether a smart mannequin system could accurately measure neck forces and moments under dynamic, real-world conditions. The findings from both laboratory and field testing affirm that the system reliably captures axial loads and motion-induced torques, making it suitable for use in biomechanical and ergonomic assessments.

Laboratory testing validated the system's calibration, with load cell readings aligning closely with a reference force gauge. This supports the system's accuracy for static and semi-static conditions. However, deviations observed at higher loads (15-40 N) suggest potential instability, likely due to strain on the sensor or mounting variability. The application of a Kalman filter mitigated this issue by improving data consistency, demonstrating the value of integrating real-time signal processing in force measurement systems.

The relationship between test conditions and neck loading was clearly evident. Straight-track testing showed that increasing vehicle speed reduced axial force, indicating greater stability and less vertical displacement. In contrast, inclined and uneven terrain introduced variable forces and moments, confirming that dynamic motion and terrain roughness directly influence cervical loading. Downhill conditions, in particular, produced sharp force peaks, consistent with gravitational acceleration effects described by Newton's Second Law.

Moment measurements showed clear distinctions across terrain types. Higher flexion and extension moments were observed during uphill motion, while downhill conditions introduced greater lateral and rotational strain. These findings align with rotational mechanics, where moment magnitude depends on both force and its application distance. However, moment sensitivity during rapid impacts (e.g., sinusoidal and parallel tracks) was reduced, suggesting that sensor placement or system damping may have dampened rotational motion, limiting measurement fidelity.

Some inconsistencies were also noted in lateral moment readings, particularly when filtered values deviated from raw data. This may be due to non-uniform load distribution or mechanical misalignment. The lack of measurable neck moments in certain high-force conditions (e.g., parallel blocks) may reflect mechanical energy absorption by the spring system, rather than a true absence of moment. These limitations highlight areas for improvement in mechanical design and sensor configuration.

Compared to prior research, such as Lin et al. [36], which focused on detailed cervical modeling using embedded sensors in 3D-printed vertebrae, the proposed system offers portability and real-time responsiveness. While Lin et al.'s method is suitable for surgical simulation and laboratory testing, it lacks applicability in field conditions. This system, in contrast, bridges that gap by offering a deployable, full-body mannequin platform for in-vehicle testing.

In summary, the smart mannequin demonstrates strong potential for evaluating neck loading across realistic terrain and motion scenarios. While the results confirm its effectiveness, certain limitations—such as reduced lateral moment sensitivity and the need for external validation—must be addressed to further improve system accuracy and reliability. These insights provide a foundation for advancing biomechanical testing technologies in transportation, workplace safety, and rehabilitation research.

4. CONCLUSIONS

This study developed and evaluated a smart mannequin system designed to measure neck forces and moments under realistic vehicle operating conditions. The results from both laboratory and field testing confirmed that the system accurately captured axial forces and motion-induced moments, validating its effectiveness as a tool for dynamic biomechanical analysis.

The mannequin demonstrated the ability to respond to a wide range of environmental conditions, including straight, inclined, sinusoidal, and uneven terrains. Its integrated load cell architecture, combined with a spring-based neck mechanism and Kalman filtering, enabled real-time data acquisition with minimal noise. The system successfully identified biomechanical loading patterns that correlate with speed, terrain irregularities, and gravitational effects.

This system provides a safe, repeatable, and ethical alternative to human testing in vehicle ergonomics, with potential applications in automotive design, workplace safety, and rehabilitation technologies. It enables researchers and engineers to assess neck loading in environments that were previously difficult to replicate without risk to human subjects.

Further development is encouraged to enhance the system's lateral sensitivity and incorporate external validation for moment measurements. Future research may also explore long-term monitoring to detect fatigue patterns or extend this approach to evaluate other anatomical regions under motion stress.

ACKNOWLEDGMENT

We would like to thank PPM Telkom University and also the Center of Excellence Smart Technology and Applied Science-Rapid Research Generator School of Applied Science Telkom University (CoE STAS-RG) for facilitating the laboratory for this research.

REFERENCES

[1] Burger, M., Ellapen, T.J., Paul, Y., Strydom, G.L. (2020). Ergonomic principles as an adjunct to the profession of biokinetics. International Quarterly of Community Health Education, 40(4): 367-373. https://doi.org/10.1177/0272684X19885493

[2] Felekoglu, B., Ozmehmet Tasan, S. (2022). Interactive

ergonomic risk mapping: A practical approach for visual management of workplace ergonomics. International Journal of Occupational Safety and Ergonomics, 28(1): 45-61. https://doi.org/10.1080/10803548.2020.1712127

[3] Alam, M.D., Khan, I.A. (2024). Relation between grip force, ergonomic interventions, and task performance: A review. International Journal on Interactive Design and Manufacturing (IJIDeM), 19: 4683-47132. https://doi.org/10.1007/s12008-024-02145-x

[4] Norasi, H., Tetteh, E., Sarker, P., Mirka, G.A., Hallbeck, M.S. (2022). Exploring the relationship between neck flexion and neck problems in occupational populations: A systematic review of the literature. Ergonomics, 65(4): 587-603. https://doi.org/10.1080/00140139.2021.1976847

[5] Jeong, S., Song, T., Kim, H., Kang, M., Kwon, K., Jeon, J.W. (2011). Human neck's posture measurement using a 3-axis accelerometer sensor. In International Conference on Computational Science and Its Applications. Berlin, Heidelberg: Springer Berlin Heidelberg, pp. 96-109. https://doi.org/10.1007/978-3-642-21934-4_9

[6] Hilmi, A.H., Hamid, A.R.A., Ibrahim, W.A.R.A.W. (2024). Human-Centered ergonomics: Advancements, challenges, and future directions in industrial and occupational settings. Malaysian Journal of Ergonomics (MJEr), 6: 90-104. https://doi.org/10.58915/mjer.v6.2024.1311

[7] Li, M., Yao, X., Aschenbrenner, D., van Eijk, D., Vink, P. (2022). Ergonomics 4.0: Human-centered procedure for ergonomic design using virtual reality prototyping. In INCOSE International Symposium, 32: 195-211. https://doi.org/10.1002/iis2.12885

[8] Rong, X., Wang, B., Ding, C., Deng, Y., Chen, H., Meng, Y., Yan, W., Liu, H. (2017). The biomechanical impact of facet tropism on the intervertebral disc and facet joints in the cervical spine. The Spine Journal, 17(12): 1926-1931. https://doi.org/10.1016/j.spinee.2017.07.009

[9] Gandhi, A.A., Kode, S., DeVries, N.A., Grosland, N.M., Smucker, J.D., Fredericks, D.C. (2015). Biomechanical analysis of cervical disc replacement and fusion using single level, two level, and hybrid constructs. Spine, 40(20): 1578-1585. https://doi.org/10.1097/BRS.0000000000001044

[10] Mattucci, S.F., Cronin, D.S. (2015). A method to characterize average cervical spine ligament response based on raw data sets for implementation into injury biomechanics models. Journal of The Mechanical Behavior of Biomedical Materials, 41: 251-260. https://doi.org/10.1016/j.jmbbm.2014.09.023

[11] Alizadeh, M., Knapik, G.G., Mageswaran, P., Mendel, E., Bourekas, E., Marras, W.S. (2020). Biomechanical musculoskeletal models of the cervical spine: A systematic literature review. Clinical Biomechanics, 71: 115-124. https://doi.org/10.1016/j.clinbiomech.2019.10.027

[12] Fanton, M., Kuo, C., Sganga, J., Hernandez, F., Camarillo, D.B. (2018). Dependency of head impact rotation on head-neck positioning and soft tissue forces. IEEE Transactions on Biomedical Engineering, 66(4): 988-999. https://doi.org/10.1109/TBME.2018.2866147

[13] Hindman, B.J., From, R.P., Fontes, R.B., Traynelis, V.C., et al. (2015). Laryngoscope force and cervical spine motion during intubation in cadavers-cadavers versus patients, the effect of repeated intubations, and the effect of type II odontoid fracture on C1-C2 motion. Anesthesiology, 123(5): 1042-1058. https://doi.org/10.1097/ALN.0000000000000830

[14] Pobereskin, L.H. (2005). Whiplash following rear end collisions: A prospective cohort study. Journal of Neurology, Neurosurgery & Psychiatry, 76(8): 1146-1151. https://doi.org/10.1136/jnnp.2004.049189

[15] Elliott, J.M., Walton, D.M., Albin, S.R., Courtney, D.M., Siegmund, G.P., Carroll, L.J., Weber II DC, K.A., Smith, A.C. (2023). Biopsychosocial sequelae and recovery trajectories from whiplash injury following a motor vehicle collision. The Spine Journal, 23(7): 1028-1036. https://doi.org/10.1016/j.spinee.2023.03.005

[16] Erbulut, D.U. (2014). Biomechanics of neck injuries resulting from rear-end vehicle collisions. Turkish Neurosurgery, 24(4). https://doi.org/10.5137/1019-5149.JTN.9218-13.1

[17] Prall, J., Ross, M. (2019). The management of work-related musculoskeletal injuries in an occupational health setting: The role of the physical therapist. Journal of Exercise Rehabilitation, 15(2): 193. https://doi.org/10.12965/jer.1836636.318

[18] Elkin, B.S., Elliott, J.M., Siegmund, G.P. (2016). Whiplash injury or concussion? A possible biomechanical explanation for concussion symptoms in some individuals following a rear-end collision. Journal of Orthopaedic & Sports Physical Therapy, 46(10): 874-885. https://doi.org/10.2519/jospt.2016.7049

[19] Mousavi-Khatir, R., Talebian, S., Toosizadeh, N., Olyaei, G.R., Maroufi, N. (2018). The effect of static neck flexion on mechanical and neuromuscular behaviors of the cervical spine. Journal of Biomechanics, 72: 152-158. https://doi.org/10.1016/j.jbiomech.2018.03.004

[20] Charles, L.E., Ma, C.C., Burchfiel, C.M., Dong, R.G. (2018). Vibration and ergonomic exposures associated with musculoskeletal disorders of the shoulder and neck. Safety and Health at Work, 9(2): 125-132. https://doi.org/10.1016/j.shaw.2017.10.003

[21] Nordander, C., Hansson, G.Å., Ohlsson, K., Arvidsson, I., Balogh, I., Strömberg, U., Rittner, R., Skerfving, S. (2016). Exposure-response relationships for work-related neck and shoulder musculoskeletal disorders-analyses of pooled uniform data sets. Applied Ergonomics, 55: 70-84. https://doi.org/10.1016/j.apergo.2016.01.010

[22] Hoe, V.C., Urquhart, D.M., Kelsall, H.L., Zamri, E.N., Sim, M.R. (2018). Ergonomic interventions for preventing work-related musculoskeletal disorders of the upper limb and neck among office workers. Cochrane Database of Systematic Reviews, 2018(10). https://doi.org/10.1002/14651858.CD008570.pub3

[23] Desai, R., Guha, A., Seshu, P. (2018). Multibody biomechanical modelling of human body response to direct and cross axis vibration. Procedia Computer Science, 133: 494-501. https://doi.org/10.1016/j.procs.2018.07.062

[24] Kim, J.H., Dennerlein, J.T., Johnson, P.W. (2018). The effect of a multi-axis suspension on whole body vibration exposures and physical stress in the neck and low back in agricultural tractor applications. Applied Ergonomics, 68: 80-89. https://doi.org/10.1016/j.apergo.2017.10.021

[25] Xu, T., Sheng, X., Zhang, T., Liu, H., Liang, X., Ding,

A. (2018). Development and validation of dummies and human models used in crash test. Applied Bionics and Biomechanics, 2018(1): 3832850. https://doi.org/10.1155/2018/3832850

[26] Atarod, M. (2020). Biomechanics of passenger vehicle underride: An analysis of IIHS crash test data (No. 2020-01-0525). SAE Technical Paper. https://doi.org/10.4271/2020-01-0525

[27] Jaśkiewicz, M., Frej, D., Matej, J., Chaba, R. (2021). Analysis of the head of a simulation crash test dummy with speed motion. Energies, 14(5): 1476. https://doi.org/10.3390/en14051476

[28] Schmitt, K.U., Muser, M.H., Thueler, H., Bruegger, O. (2018). Crash-test dummy and pendulum impact tests of ice hockey boards: Greater displacement does not reduce impact. British Journal of Sports Medicine, 52(1): 41-46. https://doi.org/10.1136/bjsports-2017-097735

[29] Tu, J., Gao, W. (2021). Ethical considerations of wearable technologies in human research. Advanced Healthcare Materials, 10(17): 2100127. https://doi.org/10.1002/adhm.202100127

[30] le Feber, M., Jadoenathmisier, T., Goede, H., Kuijpers, E., Pronk, A. (2021). Ethics and privacy considerations before deploying sensor technologies for exposure assessment in the workplace: Results of a structured discussion amongst Dutch stakeholders. Annals of Work Exposures and Health, 65(1): 3-10. https://doi.org/10.1093/annweh/wxaa093

[31] Benson, L.C., Clermont, C.A., Ferber, R. (2020). New considerations for collecting biomechanical data using wearable sensors: The effect of different running environments. Frontiers in Bioengineering and Biotechnology, 8: 86. https://doi.org/10.3389/fbioe.2020.00086

[32] Alzahrani, A., Ullah, A. (2024). Advanced biomechanical analytics: Wearable technologies for precision health monitoring in sports performance. Digital Health, 10: 20552076241256745. https://doi.org/10.1177/20552076241256745

[33] Poliak, M., Frej, D., Jaśkiewicz, M., Caban, J., Górniak, A., Gidlewski, M., Hajduk, I.E., Hajduk, I.E., Tarnapowicz, D. (2024). Analysis of head movement in KPSIT dummies and the impact of seats and seat belts during low-speed collisions 20km/h. Sensors, 24(17): 5714. https://doi.org/10.3390/s24175714

[34] Lee, W.K., Yoon, H., Han, C., Joo, K.M., Park, K.S. (2016). Physiological signal monitoring bed for infants based on load-cell sensors. Sensors, 16(3): 409. https://doi.org/10.3390/s16030409

[35] Kumar, A.A., Tewari, V.K., Nare, B. (2016). Embedded digital draft force and wheel slip indicator for tillage research. Computers and Electronics in Agriculture, 127: 38-49. https://doi.org/10.1016/j.compag.2016.05.010

[36] Lin, M., Paul, R., Liao, X., Doulgeris, J., Menzer, E.L., Dhar, U.K., Tsai, C.T., Vrionis, F.D. (2023). A new method to evaluate pressure distribution using a 3D-Printed C2-C3 cervical spine model with an embedded sensor array. Sensors, 23(23): 9547. https://doi.org/10.3390/s23239547

[37] Gao, W., Kim, S.W., Bosse, H., Haitjema, H., Chen, Y.L., Lu, X.D., Knapp, W., Weckenmann, A., Estler, W.T., Kunzmann, H. (2015). Measurement technologies for precision positioning. CIRP Annals, 64(2): 773-796. https://doi.org/10.1016/j.cirp.2015.05.009

[38] Bureneva, O., Safyannikov, N. (2022). Strain gauge measuring system for subsensory micromotions analysis as an element of a hybrid human-machine interface. Sensors, 22(23): 9146. https://doi.org/10.3390/s22239146

[39] Preethichandra, D.M.G., Piyathilaka, L., Sul, J.H., Izhar, U., Samarasinghe, R., Arachchige, S.D., de Silva, L.C. (2024). Passive and active exoskeleton solutions: Sensors, actuators, applications, and recent trends. Sensors, 24(21): 7095. https://doi.org/10.3390/s24217095

[40] Zhao, H., Jalving, J., Huang, R., Knepper, R., Ruina, A., Shepherd, R. (2016). A helping hand: soft orthosis with integrated optical strain sensors and EMG control. IEEE Robotics & Automation Magazine, 23(3): 55-64. https://doi.org/10.1109/MRA.2016.2582216

[41] Connan, M., Ruiz Ramírez, E., Vodermayer, B., Castellini, C. (2016). Assessment of a wearable force- and electromyography device and comparison of the related signals for myocontrol. Frontiers in Neurorobotics, 10: 17. https://doi.org/10.3389/fnbot.2016.00017

[42] Yoganadan, N., Humm, J., Baisden, J., Varghese, V., Banerjee, A. (2022). Human tolerance to injury under complex head-neck loading. In ASME International Mechanical Engineering Congress and Exposition. American Society of Mechanical Engineers, 86663: V004T05A042. https://doi.org/10.1115/IMECE2022-95731

[43] Ovsepyan, A.L., Smirnov, A.A., Pustozerov, E.A., Mokhov, D.E., Mokhova, E.S., Trunin, E.M., Dydykin, S.S., Vasil'ev, Y.L., Yakovlev, E.V., Budday, S., Paulsen, F., Zhivolupov, S.A., Starchik, D.A. (2022). Biomechanical analysis of the cervical spine segment as a method for studying the functional and dynamic anatomy of the human neck. Annals of Anatomy-Anatomischer Anzeiger, 240: 151856. https://doi.org/10.1016/j.aanat.2021.151856.

[44] Barrett, J.M., McKinnon, C., Callaghan, J.P. (2020). Cervical spine joint loading with neck flexion. Ergonomics, 63(1): 101-108. https://doi.org/10.1080/00140139.2019.1677944

[45] Chowdhury, S.K., Zhou, Y., Wan, B., Reddy, C., Zhang, X. (2022). Neck strength and endurance and associated personal and work-related factors. Human Factors, 64(6): 1013-1026. https://doi.org/10.1177/0018720820983635

[46] Haniffah, A.N., Dawal, S.Z., Julaihi, S. (2020). Whiplash injury mechanisms of car rear occupants: A review. Malaysian Journal of Public Health Medicine, 20(Special1): 272-281. https://doi.org/10.37268/mjphm/vol.20/no.Special1/art.708

[47] Derouin, A.J., Law, A.J., Wright Beatty, H., Wickramasinghe, V., Fischer, S.L. (2023). The effects of whole-body vibration and head supported mass on performance and muscular demand. Ergonomics, 66(1): 1-15. https://doi.org/10.1080/00140139.2022.2053589

[48] Pickard, O., Burton, P., Yamada, H., Schram, B., Canetti, E.F., Orr, R. (2022). Musculoskeletal disorders associated with occupational driving: A systematic review spanning 2006-2021. International Journal of Environmental Research and Public Health, 19(11): 6837. https://doi.org/10.3390/ijerph19116837

[49] Greggi, C., Visconti, V.V., Albanese, M., Gasperini, B.,

Chiavoghilefu, A., Prezioso, C., Persechino, B., Iavicoli, S., Gasbarra, E., Iundusi, R., Tarantino, U. (2024). Work-related musculoskeletal disorders: A systematic review and meta-analysis. Journal of Clinical Medicine, 13(13): 3964. https://doi.org/10.3390/jcm13133964

[50] O'Reilly, K., McDonnell, J.M., Ibrahim, S., Butler, J.S., Martin-Smith, J.D., O'Sullivan, J.B., Dolan, R.T. (2024). Biomechanical and ergonomic risks associated with cervical musculoskeletal dysfunction amongst surgeons: A systematic review. The Surgeon, 22(3): 143-149. https://doi.org/10.1016/j.surge.2024.04.003

[51] Torres San Miguel, C.R., Perez Valdez, J.A., Ceccarelli, M., Russo, M. (2024). The problems and design of a neck dummy. Biomimetics, 9(11): 661. https://doi.org/10.3390/biomimetics9110661

[52] Johnson, D., Koya, B., Gayzik, F.S. (2020). Comparison of neck injury criteria values across human body models of varying complexity. Frontiers in Bioengineering and Biotechnology, 8: 985. https://doi.org/10.3389/fbioe.2020.00985

[53] Miura, S., Takahashi, S., Parque, V., Miyashita, T. (2020). Small-Scale human impact anthropomorphic test device using the similarity rule. IEEE Transactions on Industrial Electronics, 68(8): 7188-7198. https://doi.org/10.1109/TIE.2020.3003590

[54] Rueda-Arreguín, J.L., Ceccarelli, M., Torres-SanMiguel, C.R. (2022). Design of an articulated neck to assess impact head-neck injuries. Life, 12(2): 313. https://doi.org/10.3390/life12020313

[55] Krašna, S., Đorđević, S. (2020). Estimating the effects of awareness on neck-muscle loading in frontal impacts with EMG and MC sensors. Sensors, 20(14): 3942. https://doi.org/10.3390/s20143942

[56] Tang, K.P.M., Yick, K.L., Li, P.L., Yip, J., Or, K.H., Chau, K.H. (2020). Effect of contacting surface on the performance of thin-film force and pressure sensors. Sensors, 20(23): 6863. https://doi.org/10.3390/s20236863

[57] Lingampally, P.K., Doss, A.S.A., Kadiyam, V.R. (2022). Wearable neck assistive device strain evaluation study on surface neck muscles for head/neck movements. Technology and Health Care, 30(6): 1503-1513. https://doi.org/10.3233/THC-220101

[58] Ammar, M.M., Mohamed, M.I., Mahmoud, G.M., Kumme, R., Zakaria, H.M., Gaafer, A.M. (2024). Identification of load cells parameters under applying creep and dynamic force for dynamic force calibrations. Measurement, 224: 113851. https://doi.org/10.1016/j.measurement.2023.113851

[59] Jarque-Bou, N.J., Sancho-Bru, J.L., Vergara, M. (2021). A systematic review of EMG applications for the characterization of forearm and hand muscle activity during activities of daily living: Results, challenges, and open issues. Sensors, 21(9): 3035. https://doi.org/10.3390/s21093035

[60] Farooq, M., Iqbal, T., Vazquez, P., Farid, N., Thampi, S., Wijns, W., Shahzad, A. (2020). Thin-film flexible wireless pressure sensor for continuous pressure monitoring in medical applications. Sensors, 20(22): 6653. https://doi.org/10.3390/s20226653

[61] Song, P., Liu, J., Wang, F., Sun, X. (2021). The study of inspection on thin film resistance strain gauge contact failure by electrical excitation thermal-wave imaging. IEEE Transactions on Industrial Electronics, 69(6): 6288-6297. https://doi.org/10.1109/TIE.2021.3088368

NOMENCLATURE

F	Applied force
m	Mass acting on the system
a	Acceleration due to vehicle motion
M	Moment of force (torque)
d	Perpendicular distance from pivot point
MEP	Mean Error Percentage
K	Kalman gain
P	Process variance
R	Measurement variance
x	Estimated (filtered) state

Subscripts

i	Index of measurement sample
$Gauge$	Measurement from force gauge
$Loadcell$	Measurement from load cell